minerals

MDPI

Article

$^{40}Ar/^{39}Ar$ Geochronology of the Malyy (Little) Murun Massif, Aldan Shield of the Siberian Craton: A Simple Story for an Intricate Igneous Complex

Alexei V. Ivanov [1,*], Nikolay V. Vladykin [2], Elena I. Demonterova [1], Viktor A. Gorovoy [1] and Emilia Yu. Dokuchits [2]

[1] Institute of the Earth's Crust, Siberian Branch of the Russian Academy of Sciences, 664033 Irkutsk, Russia; dem@crust.irk.ru (E.I.D.); vagorovoi@mail.ru (V.A.G.)

[2] A.P. Vinogradov Institute of Geochemistry, Siberian Branch of the Russian Academy of Sciences, 664033 Irkutsk, Russia; vlad@igc.irk.ru (N.V.V.); esfor@rambler.ru (E.Y.D.)

* Correspondence: aivanov@crust.irk.ru; Tel.: +7-395-242-7000

Received: 17 November 2018; Accepted: 16 December 2018; Published: 19 December 2018

Abstract: The Malyy (Little) Murun massif of the Aldan Shield of the Siberian Craton has long been a kind of Siberian Mecca for geologists. It has attracted thousands of geologists, prospectors, and mineral collectors despite its remote location. It is famous for a dozen new and rare minerals, including the gemstones charoite and dianite (the latter is the market name for strontian potassicrichrerite), as well as for a range of uncommon alkaline igneous rocks. Despite this, the age of the Malyy Murun igneous complex and associated metasomatic and hydrothermal mineral associations has remained poorly constrained until now. In this paper, we provide extensive $^{40}Ar/^{39}Ar$ geochronological data to reveal its age and temporal history. It appears that, although unique in terms of rocks and constituent minerals, the Malyy Murun is just one of multiple alkaline massifs and lavas emplaced in the Early Cretaceous (~137–128 Ma) within a framework of the extensional setting of the Aldan Shield and nearby Transbaikalian region. The extension took place 40–60 million years after the supposed closure of the Mongolia–Okhotsk Ocean and orogenic peak in the Early–Middle Jurassic.

Keywords: Malyy (Little) Murun massif; Aldan Shield; Siberian Craton; $^{40}Ar/^{39}Ar$ dating

1. Introduction

The Malyy (Little) Murun massif of the Aldan Shield of the Siberian Craton (Figure 1), though located in remote Siberia, is familiar to several generations of Russian geologists and to the international community due to a specific assemblage of alkaline igneous rocks [1–16] and mineral deposits for U, Th, Au, Pb, Ti, Sr, and Ba, associated with intrusive and post-intrusive stages of this massif [12–19]. At last, but not least, the Malyy Murun massif is famous for the only world occurrence of gemstone charoite [20–24].

In the 1980s, up to several thousand geologists and miners worked at the Malyy Murun massif during the short Siberian summers in search for various metal and non-metal resources. Today, only limited mining operations are conducted there for the gemstone market (charoite, dianite—the market name for strontian potassicrichrerite [24]), and metallurgy (Ba–Sr benstonite carbonatite [12–14]). The Malyy Murun has a high potential for mineralogists and petrologists. It is worth mentioning that a number of new minerals and mineral varieties have been discovered there (charoite [20,25], tinaksite [26,27], tokkoite [27,28], frankamenite [29,30], strontian potassicrichrerite [31,32], tausonite [33,34], murunskite [35,36], vladykinite [37]), and various exotic rocks such as lamproites, carbonatites, alkaline granites, and various syenitic rocks.

Despite the enormous efforts for understanding the geology of the Malyy Murun massif, its geochronology was constrained to Early Cretaceous by an outdated K-Ar dating of voluminously predominant syenites [38]. A few attempts were also made recently to limit the timing of the charoite mineralization by $^{40}Ar/^{39}Ar$ dating [39,40]. In this study, we provide new $^{40}Ar/^{39}Ar$ results on all major igneous and hydrothermal stages recognized in the Malyy Murun massif. We use this geochronological information to constrain the duration of magmatic and later hydrothermal activity within the massif and to compare it with the information on alkaline magmatism of the Aldan Shield of the Siberian Craton and the Transbaikalian rifted region [41–53] (Figure 1).

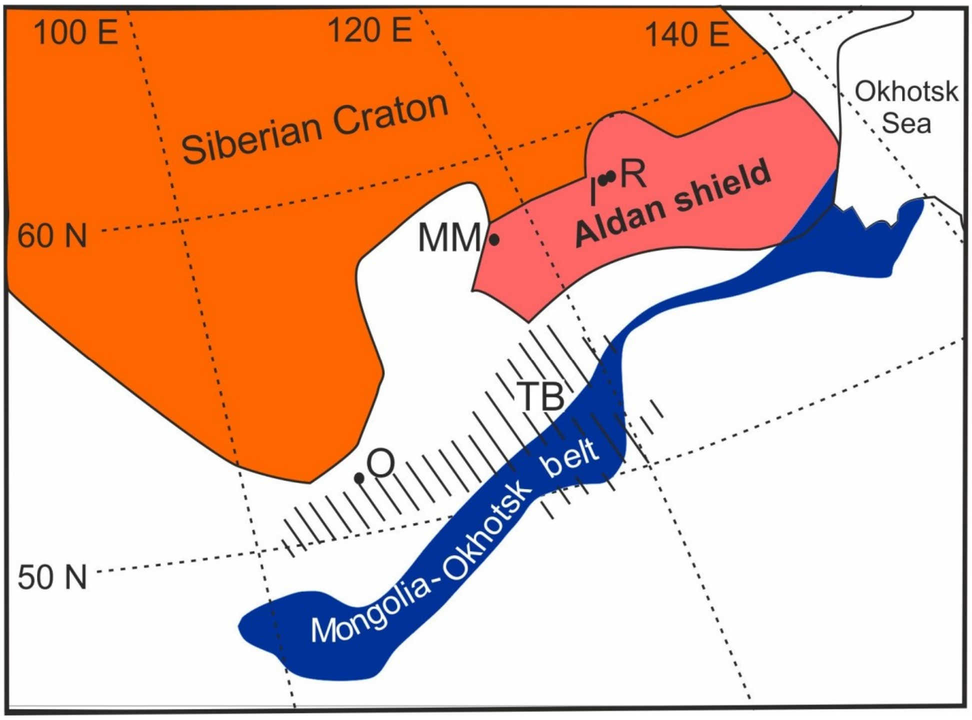

Figure 1. Location of the Malyy Murun and some other alkaline complexes in the tectonic framework of the Siberian Craton and the Mongolia–Okhotsk belt (modified after [39]). The latter is a Jurassic orogen formed due to the closure of an ocean of the same name. Aldan Shield is the cratonic basement intruded by numerous Cretaceous small volume alkaline intrusions [38]. TB (hatched) is a Transbaikalian region rifted in Cretaceous with the formation of basins and associated alkaline basaltic volcanism [45]. Acronyms: MM—Malyy Murun, I—Inagly, R—Ryabinovy, O—Oshurkov.

2. Materials and Methods

According to [15], the Malyy Murun massif can be subdivided into four igneous phases or stages (early intrusive, main intrusive, volcanic, and late intrusive). The relation between different igneous stages was not always clear because the rocks classified to one or another of the four stages are usually separated by faults, and no direct contacts can be observed for all rock types to establish the complete scheme based purely on geological relationships. Thus, it is not surprising that other subdivisions can be found in the literature (e.g., [22]). Here we follow the subdivision of [15], though we slightly modify it as indicated below.

Rocks of the early intrusive stage are predominantly located in the northeastern part of the massif (Figure 2), where they were recovered through drilling and mining of an exploratory gallery. Biotite-pyroxenites, K-ijolites, olivine lamproites, feldspar-shonkinites, leucitic shonkinites, and cumulative olivine-spinel and olivine-pyroxene-phlogopite-monticellite rocks form a layered complex. For the geochronological purpose, mica was separated from biotite-pyroxenite, olivine lamproite, and olivine-pyroxene-phlogopite-monticellite rock (Appendix A).

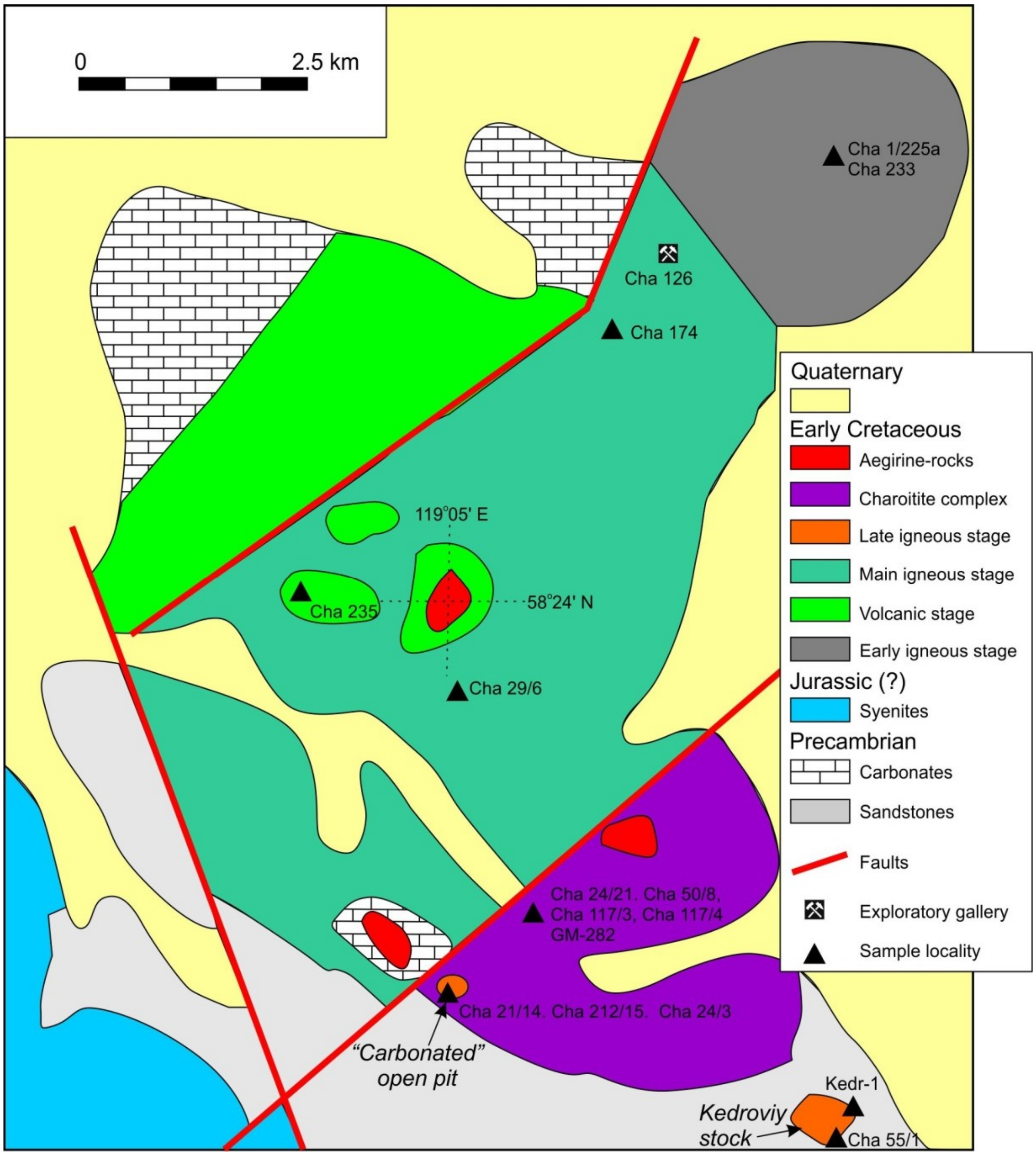

Figure 2. A schematic map of the Malyy Murun massif with the location of the studied samples.

Rocks of the main intrusive stage composed the central part of the massif (Figure 2), which consists of different types of syenites (leucitic, feldspar–calcilitic, biotite–pyroxene–K-feldspar). For $^{40}Ar/^{39}Ar$ dating, we separated mica from abundant biotite-pyroxene-K-feldspar syenite (referred to as alkaline syenite by Russian geologists).

The volcanic stage was recognized by the lava of leucitic lamproites and melaphonolites and volcanic breccia. The latter includes clasts of rocks of the main intrusive stage. Dykes of tinguaites, richterite–sanidine lamproites, trachyte–porphyries, syenite–porphyries, and (eudialyte-bearing) lujavrites were included into the volcanic stage. For $^{40}Ar/^{39}Ar$ dating, we separated mica from leucitic lamproite lava and lujavrite dyke.

According to [15], the late intrusive stage includes benstonite, calcite, and quartz–calcite carbonatites (Figure 3) and various types of silicate–carbonate rocks (with a variable content of K-feldspar, pyroxene, and calcite) spatially-associated with charoitites (Figure 4). For the purpose of this study, we kept carbonatites as the true representatives of the late intrusive stage, whilst considering other silicate–carbonate and silicate rocks (often referred to as fenites (e.g., [22])) within the charoite complex (Figure 2). In addition, we included, into the late intrusive stage, alkaline granites of spatially-separated Kedroviy stock (Figure 2), which were considered within the main intrusive stage [15] or a late stage [22]. For $^{40}Ar/^{39}Ar$ dating of the late intrusive stage, we separated tinaksite and K-feldspar from benstonite carbonatite and K-feldspar from calcite carbonatite. In order to obtain the age constraints on alkaline granites of the Kedroviy stock, we separated alkaline amphibole (strontian potassicrichterite [31]) from a metasomatic contact zone.

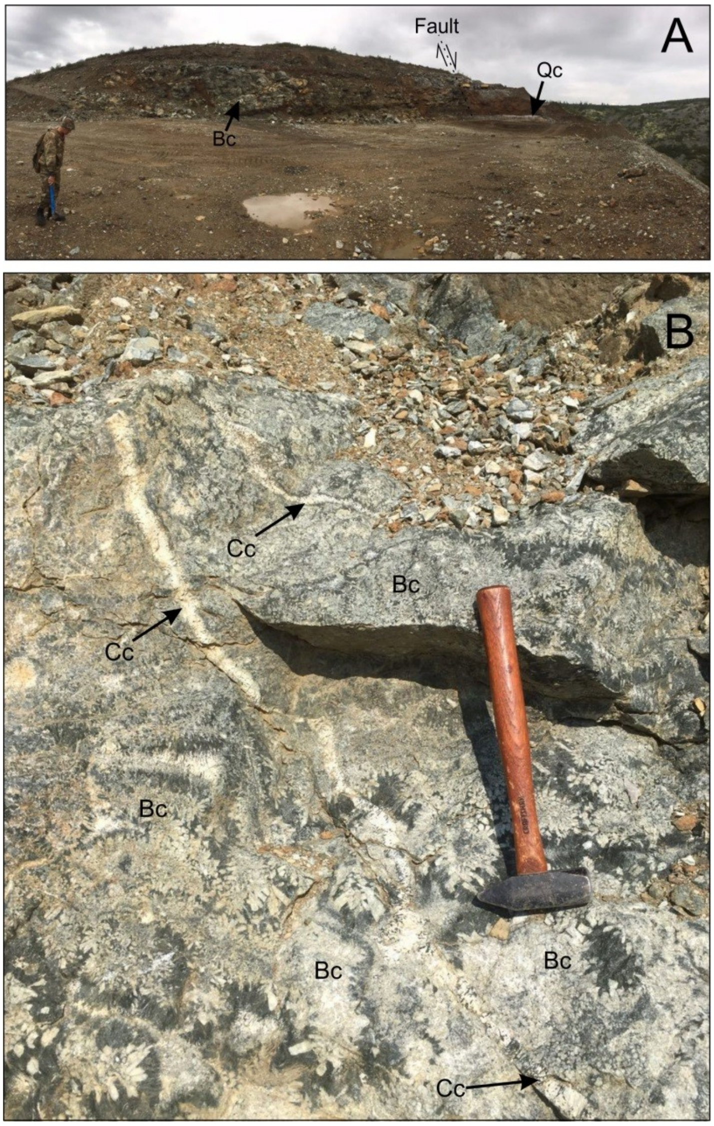

Figure 3. The "carbonated" open pit: (**A**) a general view with shown sites of benstonite carbonatite (Bc) and quartz carbonatite (Qc) blocks separated by a fault; (**B**) a close view of benstonite carbonatite (Bc) cut by calcite carbonatite (Cc) veins.

Hydrothermal activity within, and in the vicinity, of the Malyy Murun massif is represented by quartz veins, which commonly contain rutile–brookite–anatase ore-grade mineralization [19]. For $^{40}Ar/^{39}Ar$ dating, we collected K-feldspar from one of such veins within the Kedroviy stock.

For the dating of the charoitite complex, we separated K-feldspar from charoitite and K-feldspar from a microcline monomineralic vein (Figure 4). In addition to this, we used own-published data [40] for K-feldspar from a museum sample, which likely was collected from massive K-feldspar (microcline) monomineralic rock. We also collected rare minerals, such as frankamenite, tinaksite, tokkoite, and K-arvfedsonite, taken from field samples and museum collections.

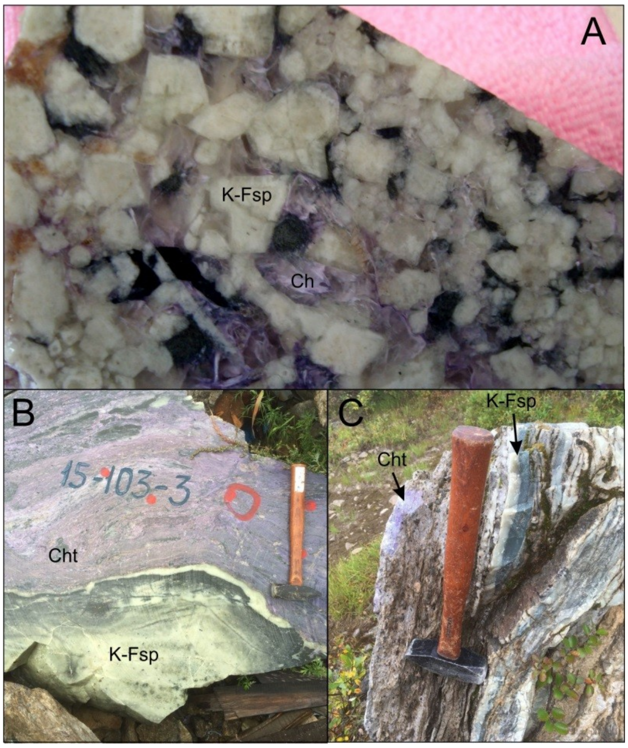

Figure 4. Different types of K-feldspar-bearing (microcline) rocks: (**A**) A polished hand specimen (~20 cm in long direction) of granular microcline (K-Fsp) in intergrowth with charoite (Ch); (**B**) a large xenolith of a massive monomineralic microcline rock (K-Fsp) within a charoitite (Cht) cut-block; (**C**) interlayering of white and dark green microcline veins (K-Fsp) with charoitite (Cht) in a natural outcrop. Reactional snow-white microcline is seen between massive microcline and charoitite in (**B**). A hammer with a 50-cm long handle is shown in (**B**,**C**) for the scale.

$^{40}Ar/^{39}Ar$ dating was performed at the Centre for Geodynamics and Geochronology at the Institute of the Earth's Crust, Siberian Branch of the Russian Academy of Sciences (Irkutsk, Russia). The analytical procedure was published elsewhere (e.g., [54]), thus only a brief description is given here. The instrument used was a noble-gas mass-spectrometer ARGUS VI (Thermo Scientific ™ (Waltham, MA, USA)) equipped with a double-vacuum resistance oven and a gas cleaning system with few SAES-getters (Lainate (Milan), Italy). Ages were calculated using the conventional decay constants [55] and a revised atmospheric $^{40}Ar/^{36}Ar$ ratio of 298.56 [56]. J-factor was derived from measurements of the BERN-4M monitor located between every 3 to 4 unknown-age samples. In order to make the $^{40}Ar/^{39}Ar$ calculated age values consistent with the U-Pb-based geochronological scale (i.e., ~1% older [57–59]), we assigned, to BERN-4M, an age of 18.885 Ma [60]. Age values were calculated using Isoplot macros for Excel [61] in a stepwise heating diagram and inverse isochron coordinates ($^{36}Ar/^{40}Ar$ vs. $^{39}Ar/^{40}Ar$). We defined a plateau as 4 or more consecutive steps within analytical error, which account for >60% of released ^{39}Ar, and whose age values overlap within an error with an age value derived by inverse isochron for the same steps. If one of the criteria above was not met, for example, 4 or more steps with <60% of released ^{39}Ar, we considered such part of the argon released spectrum as a sub-plateau, reliability of which is discussed for each case individually. If no part of the argon released spectrum could be considered as plateau or sub-plateau, we calculated the average as an approximate estimate of age. If an isochron intersects with the $^{36}Ar/^{40}Ar$ axis at a non-atmospheric ratio we preferred the isochron over the plateau. In other cases, the plateau age value was preferred as the true estimate of the emplacement age. A summary of geochronological results is provided in Appendix A. Original data are available in supplementary Table S1.

3. Results

3.1. Igneous Stages

3.1.1. Early Intrusive Stage

None of the three measured samples of the early stage intrusions yielded plateau spectrum on the argon release diagram (Figure 5). Phlogopite from the sample Cha 1/225a showed six steps within their analytical errors, with the weighted age value of 134.26 ± 0.32 Ma, and a consistent isochron age value with an atmospheric argon initial ratio. Similarly, biotites from samples Cha126 and Cha 233 showed sub-plateau age values of 133.14 ± 0.45 Ma and 135.17 ± 0.91 Ma, respectively. However, the amount of released ^{39}Ar was <60%. The obtained age values were probably partially reset.

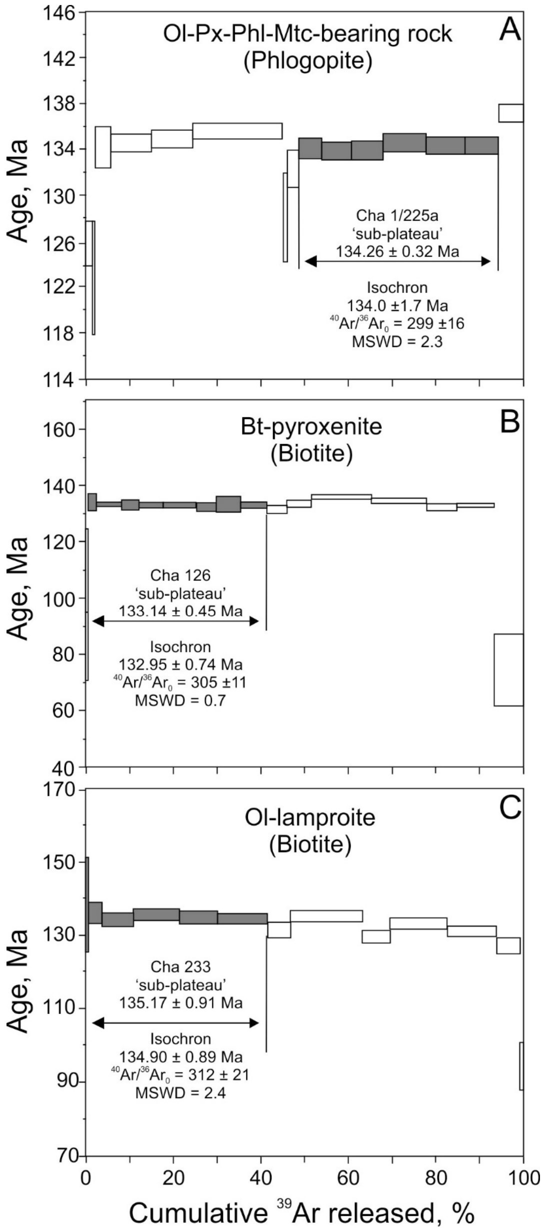

Figure 5. Argon release spectra for the early stage intrusions: (**A**) Sample Cha1/225a—cumulative olivine-pyroxene-phlogopite-monticellite rock; (**B**) sample Cha126—biotite-pyroxenite; and (**C**) sample Cha233—olivine lamproite. Steps used for calculation of sub-plateau and isochron age values are shadowed.

3.1.2. Main Intrusive and Volcanic Stages

Biotite from the volumetrically predominant biotite–pyroxene syenite (alkaline syenite according to the notion of Russian geologists) yielded a well-defined plateau with an age value of 135.76 ± 0.68 Ma, and a consistent isochron age value with an atmospheric argon initial ratio (Figure 6A). Biotite from leucite lamproite lava showed no plateau, but its argon release spectrum was flattened. We calculated an average of 142.66 ± 0.70 Ma for 13 steps, which is consistent with the isochron age value (Figure 6B). Biotite from a small lujavrite intrusion yielded a plateau age value of 136.60 ± 0.88 Ma, with a consistent isochron age value and an atmospheric isotopic composition of initially trapped argon (Figure 6C).

3.1.3. Late Intrusive Stage

K-feldspar separates from benstonite and calcite carbonatites yielded plateau age values of 128.92 ± 0.80 Ma and 129.56 ± 0.76 Ma, respectively (Figure 7A,B). These were statistically indistinguishable from each other, though calcite carbonatites cut through benstonite carbonatites (Figure 3B). Tinaksite from another benstonite carbonatite sample yielded a sub-plateau (only three steps), with a similar, though slightly older, age value of 130.93 ± 0.79 Ma (Figure 7C).

3.2. Kedroviy Stock

Strontian potassicrichrerite from the metasomatic contact of alkaline granite of the Kedroviy stock yielded a plateau with age value of 128.5 ± 1.1 Ma (Figure 8A). In inverse isochron coordinates ($^{36}Ar/^{40}Ar$ vs. $^{39}Ar/^{40}Ar$), all points plot within their errors near the $^{39}Ar/^{40}Ar$ axis, which does not allow for a linear regression to be drawn through the points. It does not affect the age calculations but prohibits the estimation of the initially-trapped argon isotope composition. We assigned this age value to the true age of the alkaline granite intrusion.

K-feldspar from a quartz-feldspar-brookite hydrothermal vein, developed in the vicinity of the Kedroviy stock, did not yield a plateau. All steps scattered near an average of 123.3 ± 0.3 Ma (Figure 8B). The isochron age value was consistent with this value and showed the atmospheric isotopic ratio for the initially-trapped argon.

3.3. Charoitite Complex

K-feldspar from different types of microcline monomineralic rocks yielded statistically different age values. For example, granular K-feldspar from association with charoite (shown in Figure 4A) yielded a well-defined plateau age value of 126.8 ± 1.1 Ma (Figure 9A). K-feldspar of a museum sample dated in our previous study [40] also showed a well-defined plateau, but with a significantly different age value of 135.79 ± 0.42 Ma (Figure 9B). This sample represented massive microclines such as shown in Figure 4B. K-feldspar from a sample of microcline veins (such as in Figure 4C) showed a slightly disturbed age spectrum with a sub-plateau age value of 129.43 ± 0.87 Ma (Figure 9C), which was intermediate between the age values obtained for the two other samples.

Tokkoite from a museum sample of charoitite yielded a plateau age value of 135.93 ± 0.49 Ma (Figure 10A), which was statistically indistinguishable from the age value obtained for K-feldspar from massive microcline monomineralic rock (Figure 9B). For the purpose of this study, we re-irradiated tokkoite from the same museum sample. It also showed a plateau, but with a slightly younger age value of 133.9 ± 1.4 Ma (Figure 10B). However, in inverse isochron coordinates the plateau steps showed the strongly non-atmospheric isotopic composition of trapped argon ($^{40}Ar/^{39}Ar$ = 184 ± 57) and, thus, the isochron age value became slightly older (135.9 ± 1.4 Ma), which was in full agreement with the age value obtained in our previous study [40].

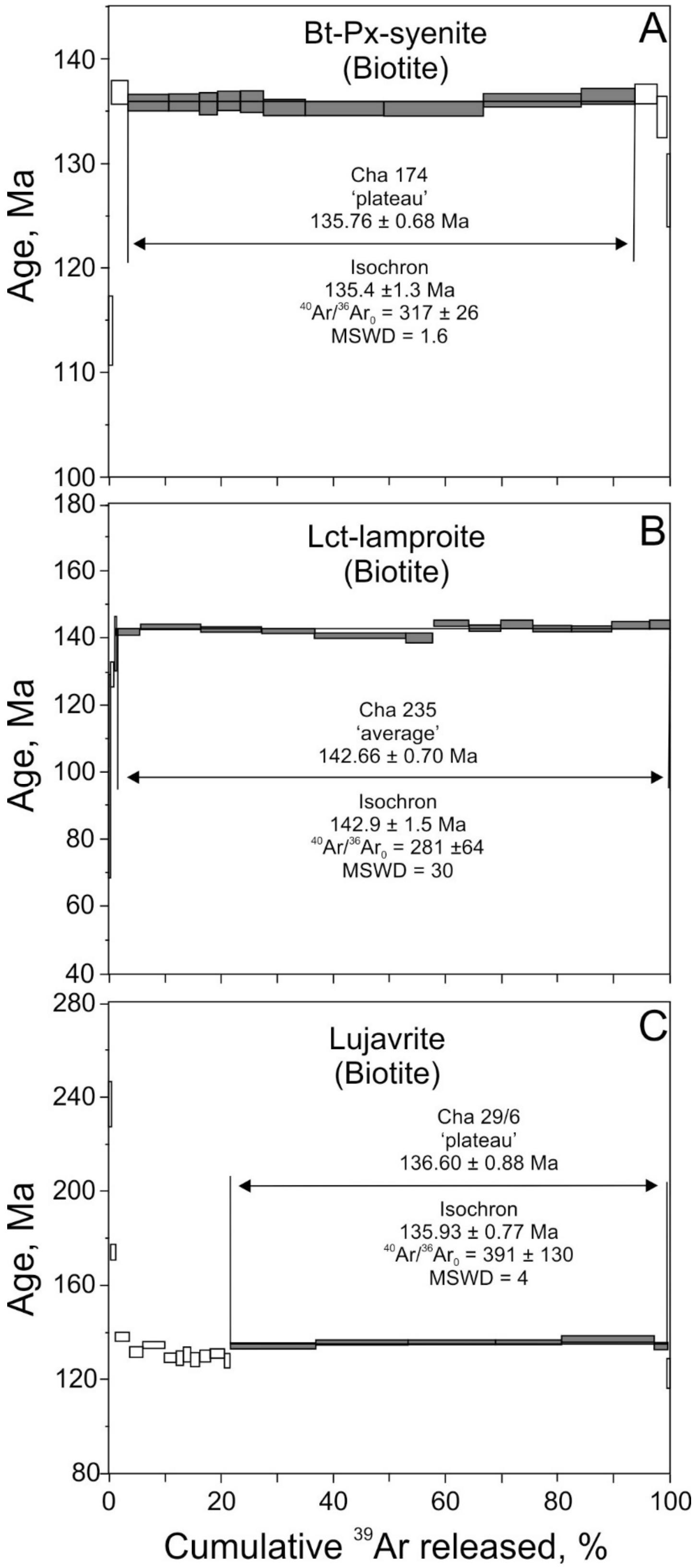

Figure 6. Argon release spectra for intrusions and lava of the main and volcanic stages: (**A**) Sample Cha174—biotite-pyroxene-syenite; (**B**) sample Cha235—leucite lamproite; and (**C**) sample Cha29/6—lujavrite. Steps used for calculation of plateau, average, and isochron age values are shadowed.

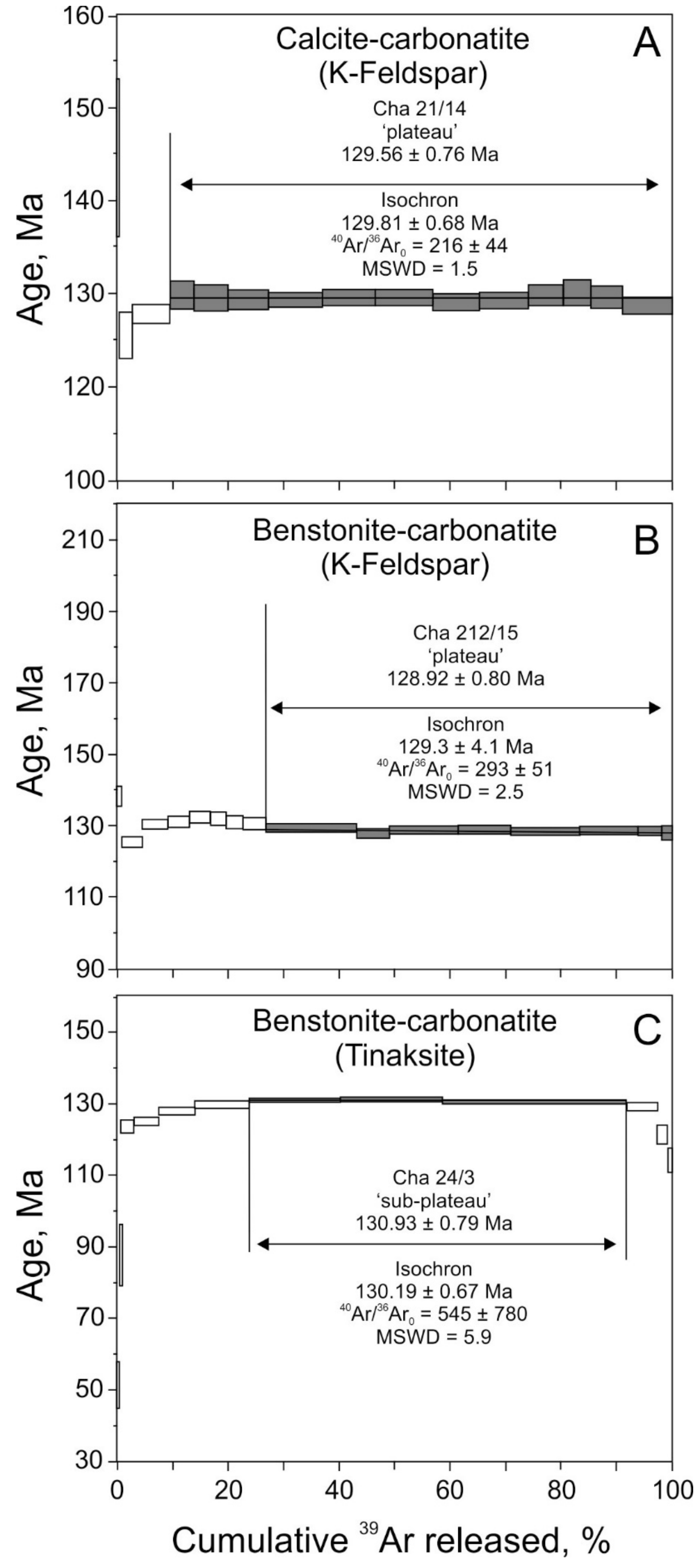

Figure 7. Argon release spectra for carbonatites of the late intrusive stage: (**A**) Sample Cha21/14—K-feldspar from calcite carbonatite; (**B**) sample Cha212/15—K-feldspar from benstonite carbonatite; and (**C**) sample Cha24/3—tinaksite ($NaK_2Ca_2TiSi_7O_{19}(OH)$) from benstonite carbonatite. Steps used for calculation of plateau, sub-plateau, and isochron age values are shadowed.

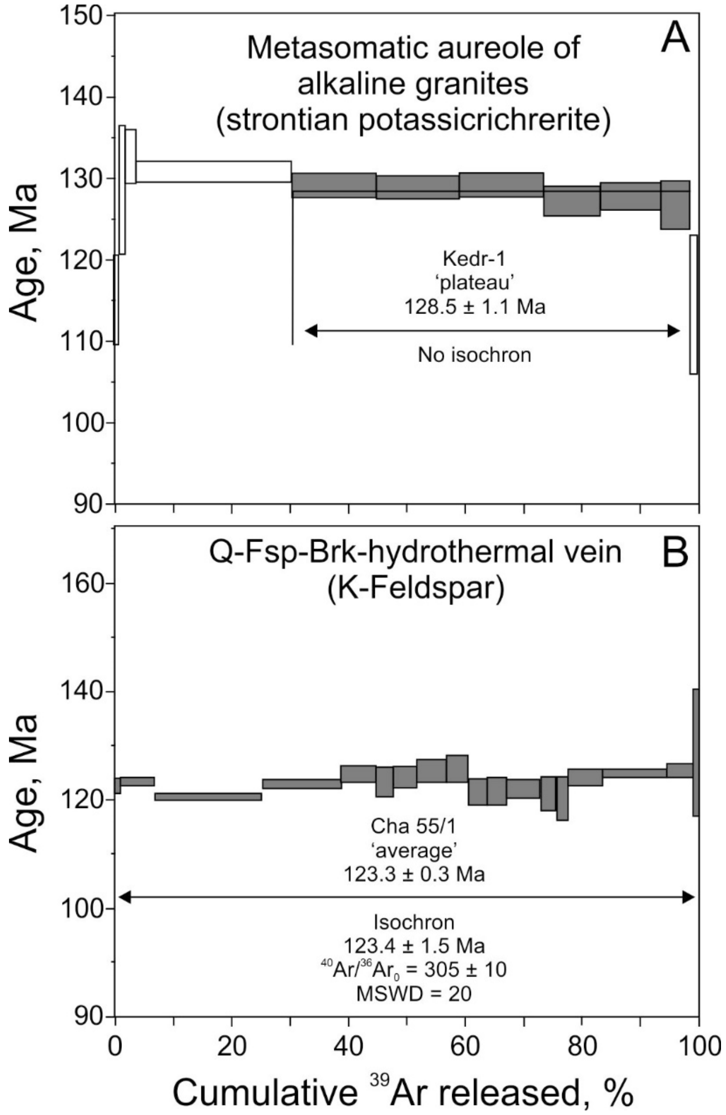

Figure 8. Argon release spectra for metasomatic and hydrothermal minerals: (**A**) Sample Kedr-1—strontian potassicrichrerite (K[(Ca,Sr)Na][Mg_5]$Si_8O_{22}(OH)_2$) in a contact zone of alkaline granite intrusion; (**B**) sample Cha55/1—K-feldspar from a quartz-feldspar-brookite hydrothermal vein. Steps used for calculation of plateau, average, and isochron age values are shadowed.

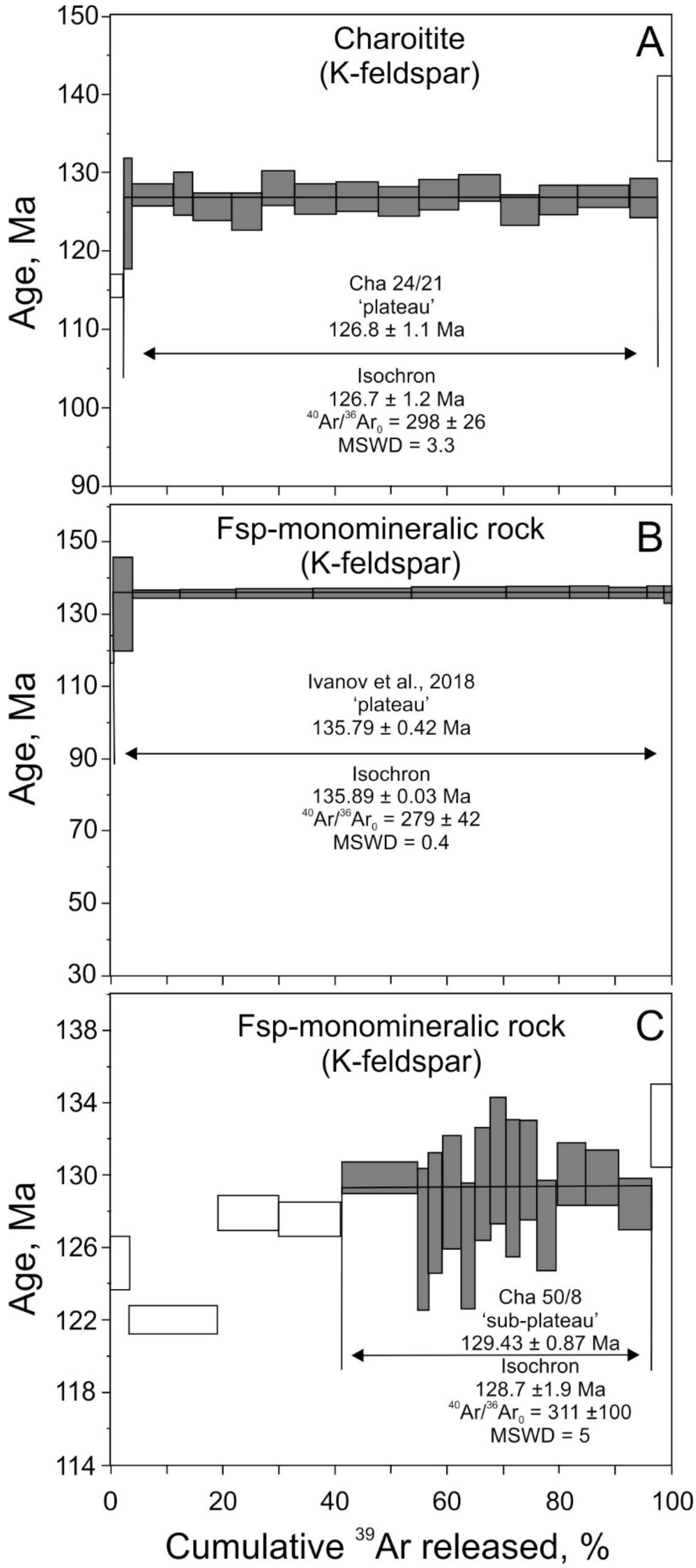

Figure 9. Argon release spectra for K-feldspar of different rocks of the charoitite complex: (**A**) Sample Cha 24/21—K-feldspar from charoitite; (**B**) museum sample of massive microclinite [40]; and (**C**) sample Cha50/8—K-feldspar from a microcline vein. Steps used for calculation of sub-plateau, plateau, and isochron age values are shadowed.

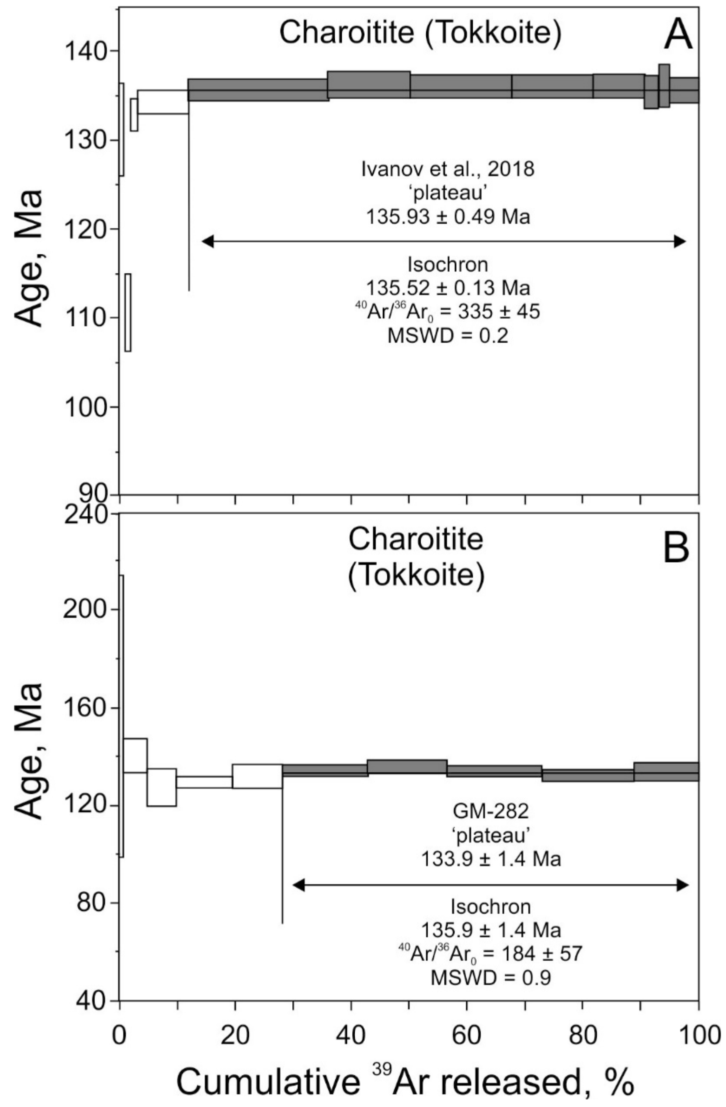

Figure 10. Argon release spectra for two different crystals of tokkoite ($K_2Ca_4Si_7O_{17}(O,OH,F)_4$) of a museum charoitite sample: (**A**) Obtained in [40] and (**B**) in this study. For the sample dated in this study, the isochron age is preferred due to the non-atmospheric trapped argon. Steps used for calculation of plateau and isochron age values are shadowed.

Tinaksite from a museum sample of charoitite analyzed in the study [40] yielded a plateau age value of 135.86 ± 0.43 Ma (Figure 11A), which was in full agreement with age values on K-feldspar from massive microcline monomineralic rock (Figure 9B) and tokkoite (Figure 10A,B). Large errors for the isotopic composition of initially-trapped argon were due to the location of all points close to the x-axis ($^{39}Ar/^{40}Ar$) of the inverse isochron plot.

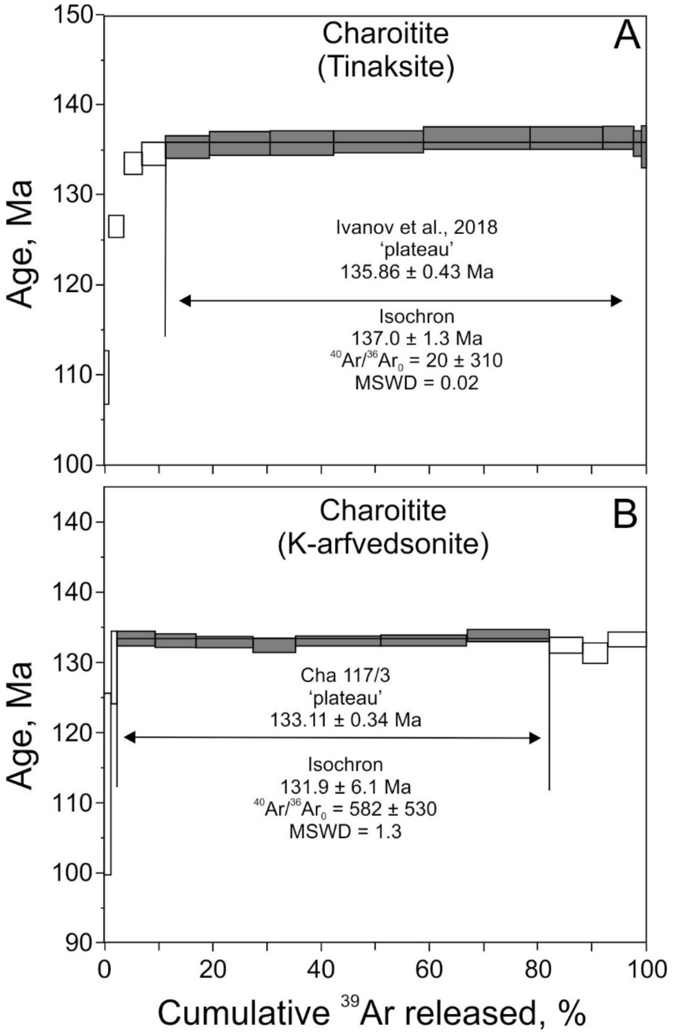

Figure 11. Argon release spectra for two different minerals of charoitites: (**A**) Tinaksite ($NaK_2Ca_2TiSi_7O_{19}(OH)$) of a museum charoitite sample analyzed in [40]; and (**B**) K-arfvedsonite analyzed in this study. Steps used for calculation of plateau and isochron age values are shadowed.

K-arfvedsonite of a charoitite sample Cha117/3 yielded a well-defined plateau with a age value of 133.11 ± 0.34 Ma (Figure 11B), which was intermediate between a few age values at about 136 Ma for tinaksite and tokkoite, and an age value of ~126 Ma obtained for granular K-feldspar in association with charoite.

Frankamenite of a museum charoitie sample analyzed in [40] yielded a sub-plateau age value of 137.55 ± 0.46 Ma (Figure 12A), which, so far, was the oldest among age values obtained for minerals of the charoitite complex. Frankamenite from the same sample reanalyzed in this study showed a similar argon-release pattern; however, no steps could be grouped as either plateau or sub-plateau. The oldest measured age value for a single step of this sample was 133.95 ± 0.77 Ma (Figure 12B). Frankamenite of another charoitite sample yielded a sub-plateau age value of 135.1 ± 1.7 Ma (Figure 12C).

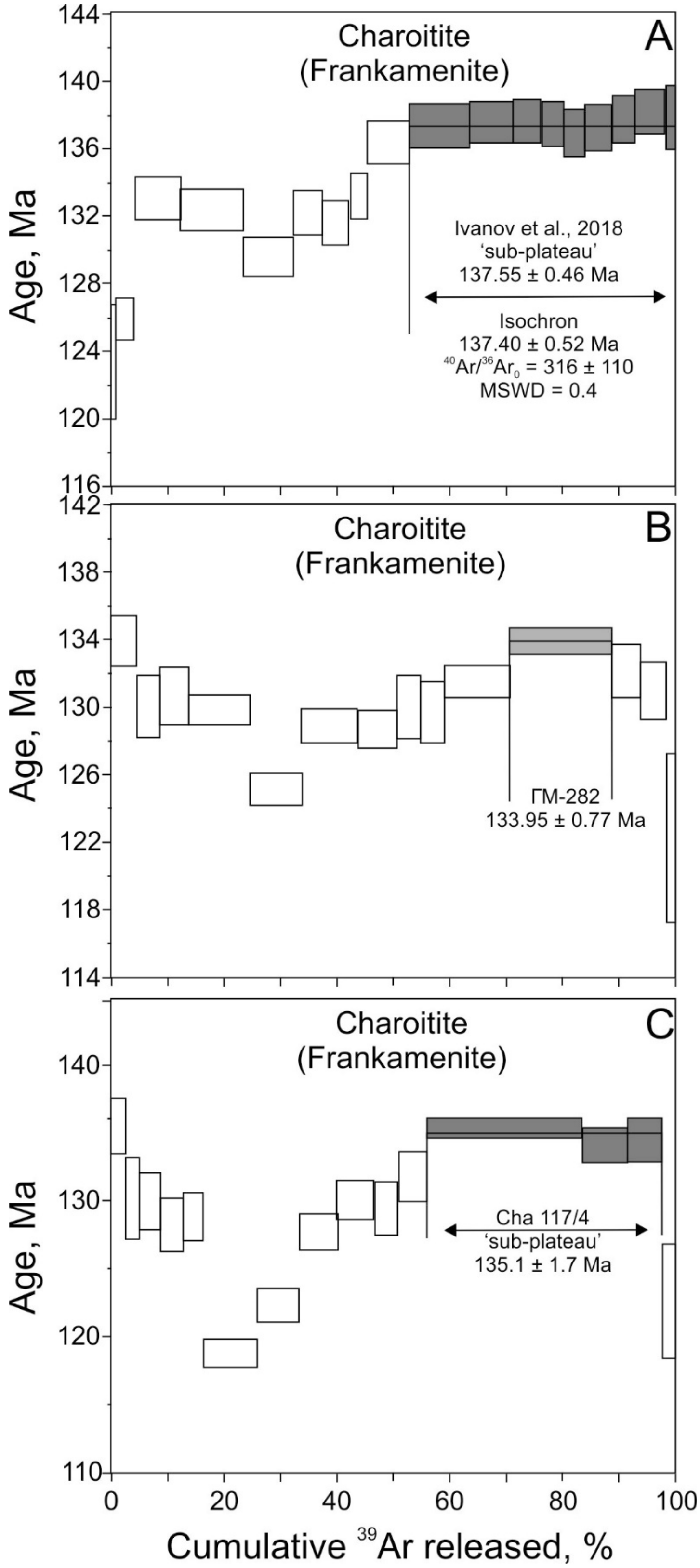

Figure 12. Argon release spectra for frankamenite ($Ca_5Na_3K_3(Si_{12}O_{30})F_3OH{\cdot}nH_2O$) crystals of two different charoitite samples: (**A**) Obtained in [40], (**B**) frankamenite from the same museum sample reanalyzed in this study; and (**C**) frankamenite from another sample Cha 117/4. Steps used for calculation of sub-plateau and single step age values are shadowed.

4. Discussion

4.1. The Timing of the Cretaceous Alkaline Magmatism of the Aldan Shield and Transbaikalia

The age of the Malyy Murun magmatism was considered as the Early Cretaceous based on K-Ar dating of biotite, K-feldspar, and pyroxene separates from feldspar–calcilitic and biotite–pyroxene–K-feldspar (referred to as alkaline) syenites of the main intrusive stage [38]. Using original data from [38] and conventional ^{40}K decay constants [42], Wang et al. [39] recalculated the mean age value for syenites of the main stage as 131 ± 2.4 Ma, excluding a few age values, which they considered as outliers. This mean age value is younger than the new ^{40}Ar/^{39}Ar age value (135.76 ± 0.68 Ma) obtained for the main stage biotite–pyroxene–K-feldspar syenite, even considering the systematic difference of the order of 0.9% between ages by [39] and this study due to different ^{40}K decay constants used. We give the priority in the interpretation of the geochronological data to our new, precise, and more accurate ^{40}Ar/^{39}Ar results over the refined K-Ar results of [38,39].

In this study, we clearly see, at least, two episodes of magmatism within the Malyy Murun massif defined by the plateau age values: ~135–137 Ma, for the main intrusive and volcanic stages, and ~128–130 Ma, for the late intrusive stage (Figure 13). The former is mainly composed of variable syenites. The latter is represented by low volume carbonatitic and alkaline granitic intrusions. With the present number of dated samples; however, it is impossible to conclude if these were two separate episodes of magmatism, or if there was continuous magmatic activity between 137 and 128 Ma. For example, the rocks of the presumably early intrusive stage may indeed be younger than the main phase syenites, or they could be reset by the main stage syenites and later intrusions (Figure 13). It also cannot be excluded that similar rocks could form during different episodes of the igneous complex development. We cannot determine, either, if magmatism started at about 137 Ma or earlier, having in mind an older (~142 Ma) age value for pseudo-leucite lamproite lava (Figure 13).

The Early Cretaceous alkaline magmatism, and associated ore deposits, were widespread within the Aldan Shield of the Siberian Craton and its surrounding along the Mongolia–Okhotsk suture zone (Figure 1). This magmatism and ore formation mark the post-collisional extension, which occurred 40–60 million years after the supposed closure of the Mongolia–Okhotsk Ocean and peak of orogeny in the Early–Middle Jurassic (e.g., [41,42]). For example, available Rb-Sr, ^{40}Ar/^{39}Ar, and U-Pb age values for Transbaikalian volcanic rocks limit the Early Cretaceous rift-related volcanism to an interval of 133–104 Ma [43–46], whereas K-Ar age values suggest a wider age interval of 150–100 Ma [47,48]. Oshurkov massif is the best studied in Transbaikalia (Figure 1). It contains granites, syenites, gabbro and lamprohyric rocks, and carbonatites [44]. The oldest among them is leucocratic granite (132.8 ± 0.66 Ma by U-Pb SHRIMP on zircon), the youngest is granitic pegmatite (111.6 ± 1 Ma by ^{40}Ar/^{39}Ar on amphibole), with numerous ages obtained by Rb-Sr, ^{40}Ar/^{39}Ar, and U-Pb methods for other rock types in between these two [44].

Similarly, according to K-Ar dating, there was the Early Cretaceous alkaline magmatism within the Aldan Shield, which was also linked to rifting [38], though there were no rift basins developed. However, ^{40}Ar/^{39}Ar and U-Pb studies are rare for the Early Cretaceous alkaline intrusives of the Aldan Shield. It seems that alkaline massifs located in the northern part of the Aldan Shield are coeval; Malyy Murun—137–128 Ma (this study); Inagly—142–128 Ma [49]; Ryabinovy—142–133 Ma [50]. Whereas, volcanic fields and intrusions located in the southern and eastern part of the Aldan shield are generally younger and fall into an interval of 126–115 Ma [51–53]. But such generalization needs additional geochronologic studies.

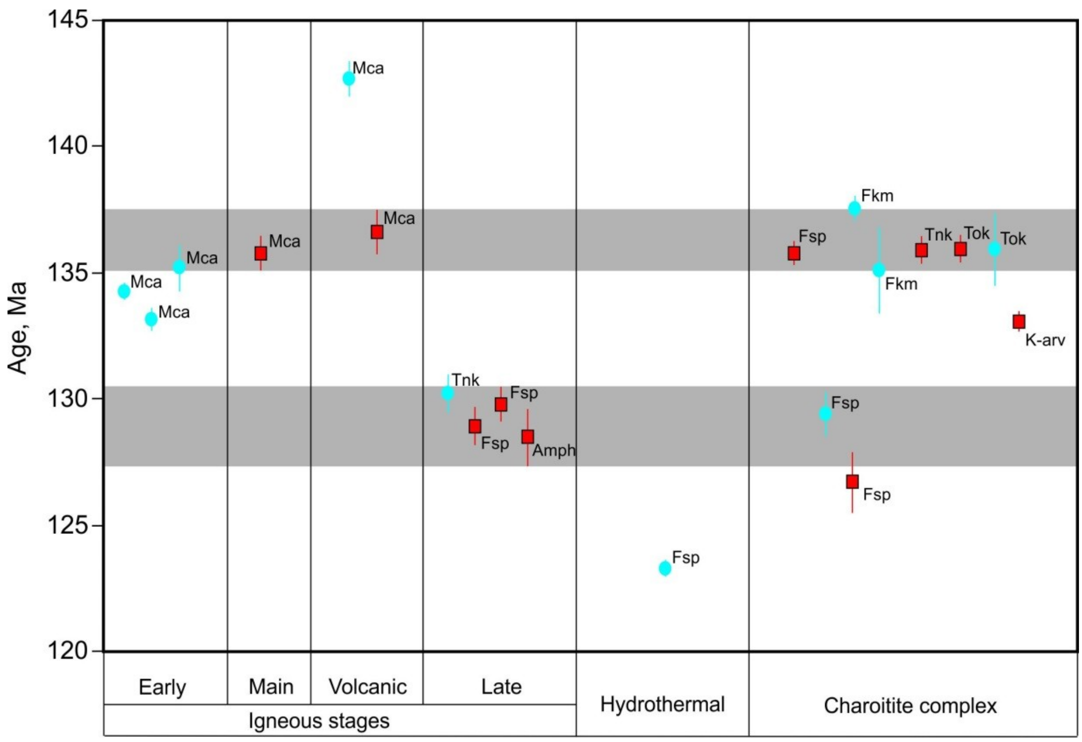

Figure 13. Summary of $^{40}Ar/^{39}Ar$ age values for the Malyy Murun massif (see Appendix A). Red squares and blue circles denote the plateau and sub-plateau/isochron age values, respectively. Horizontal grey bands show the reliably-dated intervals of igneous activity within the Malyy Murun massif. Abbreviations for dated minerals: Mca—mica (biotite in most cases and phlogopite for some early stage intrusions), Fsp—K-feldspar, Amph—amphibole (strontian potassicrichrerite), Tnk—tinaksite, Tok—tokkoite, Fkm—frankamenite, K-arv—K-arvfedsonite.

4.2. The Charoitite Complex

The charoitite complex contains a number of unique and rare minerals, which either were not discovered anywhere else (i.e., charoite, tokkoite, frankamenite) or only were found at one or two other world localities (i.e., tinaksite and fedorite). The general opinion is that the charoitite complex is metasomatic in origin [62]. However, the alternative point of view is that charoitite is of magmatic origin and associated with the evolution of lamproite and carbonatite melts [14,15].

Direct $^{40}Ar/^{39}Ar$ dating of charoite has shown that this mineral does not retain radiogenic argon due to its fibrous structure, and thus its age was assessed indirectly by laser ablation $^{40}Ar/^{39}Ar$ dating on associated K-feldspar and tinaksite [39]. Individual laser ablation analyses revealed a set of age values from 134.1 ± 2.9 Ma to 113.3 ± 3.4 Ma for K-feldspar and from 133.0 ± 3.0 Ma to 115.7 ± 4.3 Ma for tinaksite [39]. The oldest and youngest ages have been interpreted as the true crystallization ages and the time for cessation of hydrothermal activity, respectively. In the present and a related study [40], we applied stepwise-heating $^{40}Ar/^{39}Ar$ dating on K-feldspar, tinaksite, tokkoite, frankamenite, fedorite, and K-arvfedsonite. Fedorite has shown a staircase argon release pattern with significant radiogenic argon loss similar to charoite (and due to such effect is not discussed here). Frankamenite has shown disturbed age spectra (Figure 12). All other minerals have shown plateau age values (Figures 9–11), which vary from ~136 Ma to ~127 Ma (Figure 13). Thus, the charoitite complex was not formed at once. Its constituent minerals crystallized during the entire range of the Malyy Murun magmatism.

The geochronological data alone do not provide the final word in the discussion of metasomatic versus magmatic origin of charoitites. We wish to note; however, that the prolonged crystallization of minerals of charoitites would, rather, be more consistent with the interpretation of the charoitite complex, as fenites originated due to an interaction of alkalic magma fluid with carbonate and clastic sedimentary rocks [63].

The hydrothermal activity was dated via analyzing K-feldspar from the quartz-feldspar-brookite vein of the Kedroviy stock [19]. This K-feldspar did not yield a plateau, but its flattened argon release pattern suggests that it crystallized around 123 Ma (Figure 8B). The hydrothermal activity could last even longer, until ~113 Ma, as suggested by laser ablation $^{40}Ar/^{39}Ar$ dating of K-feldspar and tinaksite for the charoitite complex [39].

For example, high-temperature alteration at the Ryabinovy massif lead to crystallization of aegirine-bearing K-feldspar rock, which was dated by U-Pb SHRIMP on recrystallized zircon to 132 ± 2 Ma, whereas the intrusive phases at this massif were dated to 142–133 Ma [50]. The ore-related metasomatic alteration within Ryabinovy massif continued until 122 Ma [50].

5. Conclusions

The Malyy Murun massif was formed at about 137–128 Ma and it was just one of many alkaline intrusive massifs and lavas emplaced in the Early Cretaceous within the extensional tectonic framework of the Aldan Shield and Transbaikalia.

The unique and rare minerals of the charoitite complex were not crystallized at once. Their $^{40}Ar/^{39}Ar$ age values are fully consistent with the range of age values obtained for igneous rocks of the Malyy Murun massif.

The hydrothermal activity within the Malyy Murun massif, which played an important role in remobilization of ore components, continued for several million years after the cessation of the igneous activity.

Supplementary Materials: The following are available online at http://www.mdpi.com/2075-163X/8/12/602/s1, Table S1: $^{40}Ar/^{39}Ar$ data.

Author Contributions: Methodology, investigation, data curation, funding acquisition, project administration, and writing—original draft preparation, A.V.I.; resources, investigation, funding acquisition, and project administration, N.V.V.; investigation, project administration, and writing—original draft preparation, E.I.D.; data curation and investigation, V.A.G.; investigation and resources, E.Y.D.

Funding: The geochronological work was supported by a joint grant of the Russian Foundation for Basic Research and the Administration of the Irkutsk Region (no. 17-45-388067), given to A.V.I., E.I.D., V.A.G. and N.V.V. Sample collection and preparation were conducted under financial aid from grants of the Russian Foundation for Basic Research no. 17-55-45028 and no. 18-05-00073, given to N.V.V. and E.Y.D.

Acknowledgments: We thank Pavel Lomyga for providing useful geological information and Mikhail Mitichkin and Larisa Ivanova for support with museum sample collections.

Conflicts of Interest: The authors declare no conflict of interest.

Appendix A

Table A1. Summary of Geochronological Results.

Rock Name/Intrusive Stage, Complex	Dated Mineral	Preferred $^{40}Ar/^{39}Ar$ age Value
Olivine-pyroxene-phlogopite-monticellite rocks/Early intrusive stage	Phlogopite	134.26 ± 0.32 Ma (sub-plateau)
Biotite-pyroxenite/Early intrusive stage	Biotite	133.14 ± 0.45 Ma (sub-plateau)
Olivine-lamproites/Early intrusive stage	Biotite	135.17 ± 0.91 Ma (sub-plateau)
Biotite-pyroxene-syenite (alkaline syenite)/Main intrusive stage	Biotite	135.76 ± 0.68 Ma (plateau)
[1] Leucite-lamproite/Volcanic stage	Biotite	142.66 ± 0.70 Ma (average)
Lujavrite/Volcanic stage	Biotite	136.60 ± 0.88 Ma (plateau)
Calcite-carbonatite/Late intrusive stage	K-feldspar	129.56 ± 0.76 Ma (plateau)
Benstonite-carbonatite/Late intrusive stage	K-feldspar Tinaksite	128.92 ± 0.80 Ma (plateau) 130.93 ± 0.79 Ma (sub-plateau)
Alkaline granite/Late intrusive stage	Strontian potassicrichterite	128.5 ± 1.1 Ma (plateau

Table A1. *Cont.*

Rock Name/Intrusive Stage, Complex	Dated Mineral	Preferred $^{40}Ar/^{39}Ar$ age Value
Charoitite/Charoitite complex	K-feldspar	126.8 ± 1.1 Ma (plateau)
	Tokkoite	135.93 ± 0.49 Ma (plateau)
	Tokkoite	135.9 ± 1.4 Ma (isochron)
	Tinaksite	135.86 ± 0.43 Ma (plateau)
	K-arfvedsonite	133.11 ± 0.34 Ma (plateau)
	Frankamenite	137.55 ± 0.46 Ma (sub-plateau)
	Frankamenite	135.1 ± 1. 7 Ma (sub-plateau)
	Frankamenite	133.95 ± 0.77 Ma (oldest step)
Microcline monomineralic rock/Charoitite complex	K-feldspar	135.79 ± 0.42 Ma (plateau)
	K-feldspar	129.43 ± 0.87 Ma (sub-plateau)
Quartz-feldspar-brookite-vein	K-feldspar	123.3 ± 0.3 (average)

[1] Leucite in all rocks is recrystallized and identified by its crystal morphology.

References

1. Vladykin, N.V. 1ST occurrence of lamproites in the USSR. *Doklady Akademii Nauk SSSR* **1985**, *280*, 718–722.
2. Prokofev, V.Y.; Vorobiov, E.I. P-T conditions of formation of the Sr-Ba carbonatites, chariots, and torgolites of Murunsky alkaline massif (Eastern Siberia). *Geochimiya* **1991**, *10*, 1444–1452.
3. Mitchell, R.H.; Smith, C.B.; Vladykin, N.V. Isotopic composition of strontium and neodymium in potassic rocks of the Little Murun complex, Aldan Shield, Siberia. *Lithos* **1994**, *32*, 243–248. [CrossRef]
4. Panina, L.I. Low-titanium Aldan lamproites (Siberia): Melt inclusions in minerals. *Geoloiya i Geofizika* **1997**, *38*, 112–122.
5. Konev, A.A.; Feoktistov, G.D. Genesis of ultrasilicic alkaline granitoids. *Petrology* **1998**, *6*, 62–69.
6. Panina, L.I.; Usol'tseva, L.M. The role of liquid immiscibility of calcitic carbonatites from the Malyi Murun Massif (Aldan). *Geoloiya i Geofizika* **2000**, *41*, 655–670.
7. Vladykin, N.V. The Malyi Murun volcano-plutonic complex: An example of differentiated mantle magmas of lamproitic type. *Geochem. Int.* **2000**, *38*, S73–S83.
8. Sokolov, S.V.; Sidorenko, G.A.; Chukanov, N.V.; Chistyakova, N.I. On benstonite and benstonite carbonatites. *Geochem. Int.* **2001**, *39*, 1218–1229.
9. Davies, G.R.; Stolz, A.J.; Mahotkin, I.L.; Nowell, G.M.; Pearson, D.G. Trace element and Sr-Pb-Nd-Hf isotope evidence for ancient, fluid-dominated enrichment of the source of Aldan shield lamproites. *J. Petrol.* **2006**, *47*, 1119–1146. [CrossRef]
10. Markl, G.; Marks, M.A.W.; Frost, B.R. On the controls of oxygen fugacity in the generation and crystallization of peralkaline melts. *J. Petrol.* **2010**, *51*, 1831–1847. [CrossRef]
11. Reguir, E.P.; Chakhmouradian, A.R.; Pisiak, L.; Halden, N.M.; Yang, P.; Xu, C.; Kynicky, J.; Coueslan, C.G. Trace-element composition and zoning in clinopyroxene- and amphibole-group minerals: Implications for element partitioning and evolution of carbonatites. *Lithos* **2012**, *128*, 27–45. [CrossRef]
12. Vorob'ev, E.I. Strontium-barium carbonatites of the Murun massif (Eastern Siberia, Russia). *Geol. Ore Depos.* **2001**, *43*, 468–480.
13. Vladykin, N.V.; Tsaruk, I.I. Geology, chemistry, and genesis of Ba-Sr-bearing ("benstonite") carbonatites of the Murun Massif. *Geoloiya i Geofizika* **2003**, *44*, 325–339.
14. Vladykin, N.V.; Viladkar, S.G.; Miyazaki, T.; Mohar, V.R. Geochemistry of benstonite and associated carbonatites of Sevathur, Jogipatti and Samalpatti, Tamil Nadu, South India and Murun Massif, Siberia. *J. Geol. Soc. India* **2008**, *72*, 312–324.
15. Vladykin, N.V. Potassium alkaline lamproite-carbonatite complexes: Petrology, genesis, and ore reserves. *Russ. Geol. Geophys.* **2009**, *50*, 1119–1128. [CrossRef]
16. Vladykin, N.V. Genesis and crystallization of ultramafic alkaline carbonatite magmas of Siberia: Ore potential, mantle sources, and relationship with plume activity. *Russ. Geol. Geophys.* **2016**, *57*, 698–712. [CrossRef]
17. Borisenko, A.S.; Borovikov, A.A.; Vasyukova, E.A.; Pavlova, G.G.; Ragozin, A.L.; Prokop'ev, I.R.; Vladykin, N.V. Oxidized magmatogene fluids: Metal-bearing capacity and role of ore formation. *Russ. Geol. Geophys.* **2011**, *52*, 144–164. [CrossRef]

18. Makar'ev, L.B.; Mironov, Y.B.; Kukharenko, E.A.; Sharpenok, L.N. Breccias formation in Mesozoic ultrapotassic alkaline rocks of the Murunsky magmatic cluster (Northern Transbaikal). *Reg. Geol. Met.* **2016**, *66*, 45–52.
19. Borovikov, A.A.; Vladykin, N.V.; Tretiakova, I.G.; Dokuchits, E.Y. Physicochemical conditions of formation of hydrothermal mineralization on the Murunskiy alkaline massif, western Aldan (Russia). *Ore Geol. Rev.* **2018**, *95*, 1066–1075. [CrossRef]
20. Rogova, V.P.; Rogov, Y.G.; Drits, V.A.; Kuznetsova, N.I. Charoite—A new mineral and new jewelry-stone. *Zapiski Vsesoyuznogo Mineralogicheskogo Obshchestva* **1978**, *1*, 94–100. [CrossRef]
21. Konev, A.A.; Vorobyev, E.I.; Lazebnik, K.A. *Mineralogy of the Murun Alkaline Massif*; NITS OIGGIM: Novosibirsk, Russia, 1996; pp. 1–221. ISBN 5-7692-0006-5.
22. Vorobyev, E.I. *Charoite*; Academic Publisher "GEO": Novosibirsk, Russia, 2008; pp. 1–140. ISBN 978-5-9747-0116-0.
23. Shevelev, A.S. (Ed.) *Charoite. Violet marvel of Siberia*, 2nd ed.; Petrographica: Irkutsk, Russia, 2013; pp. 1–191. ISBN 978-5-4337-0013-0.
24. Shevelev, A.S. *Baikalian Gemstones. An Illustrated Science-Popular Publication*; Petrographica: Irkutsk, Russia, 2017; pp. 1–176. ISBN 978-5-9908900-6-0.
25. Rozhdestvenskaya, I.; Mugnaioli, E.; Czank, M.; Depmeier, W.; Kolb, U.; Reinholdt, A.; Weirich, T. The structure of charoite, $(K,Sr,Ba,Mn)_{15-16}(Ca,Na)_{32}[(Si_{7}0(O,OH)_{180})](OH,F)_{4.0}$*$nH_2O$, solved by conventional and automated electron diffraction. *Mineral. Mag.* **2010**, *74*, 159–177. [CrossRef]
26. Rogov, Y.G.; Rogova, V.P.; Voronkov, A.A.; Moleva, V.A. Tinaksite $NaK_2Ca_2TiSi_7O_{19}(OH)$—A new mineral. *Doklady Akademii Nauk SSSR* **1965**, *162*, 658–661.
27. Lacalamita, M.; Mesto, E.; Kaneva, E.; Scordari, F.; Pedrazzi, G.; Vladykin, N.; Schingaro, E. Structure refinement and crystal chemistry of tokkoite and tinaksite from the Murun massif (Russia). *Mineral. Mag.* **2017**, *81*, 251–272. [CrossRef]
28. Lazebnik, K.A.; Nikishova, L.V.; Lazebnik, Y.D. Tokkoite a new mineral of charoitites. *Mineralogicheskii Zhurnal* **1986**, *8*, 85–89.
29. Nikishova, L.V.; Lazebnik, K.A.; Rozhdestvenskaya, I.V.; Emel'yanova, N.N.; Lazebnik, Y.D. Frankamenite $K_2Na_3Ca_5(Si_{12}O_{30})F_3(OH)H_2O$—A new mineral, triclinic variety of canasite from charoitites. *Zapiski Vsesoyuznogo Mineralogicheskogo Obschestva* **1996**, *CXXV*, 106–108.
30. Rozhdestvenskaya, I.V.; Nikishova, L.V.; Lazebnik, K.A. The crystal structure of frankamenite. *Mineral. Mag.* **1996**, *60*, 897–905. [CrossRef]
31. Konev, A.A.; Paradina, L.F.; Vorob'ev, E.I.; Malyshonok, Y.V.; Lapides, I.L.; Uschapovskaya, Z.F. Magnesiumstrontian poassicricterite—A new variety of amphiboles. *Mineralogicheskii Zhurnal* **1988**, *10*, 76–82.
32. Sokolova, E.V.; Kabalov, Y.K.; McCammon, C.; Schneider, J.; Konev, A.A. Cation partitioning in an unusual strontian potassicrichterite from Siberia: Rietveld structure refinement and Mossbauer spectroscopy. *Mineral. Mag.* **2000**, *64*, 19–23. [CrossRef]
33. Afonina, G.G.; Sapozhnikov, A.N.; Vorobiev, E.I.; Konev, A.A.; Maishonok, I.V. The X-ray characteristics of tausonite, a new mineral of perovskite group. *Acta Cristal. Sect. A* **1984**, *40*, C249. [CrossRef]
34. Mitchell, R.H.; Vladykin, N.V. Rare-earth element-bearing tausonite and potassium barium titanites from the Little Murun potassic alkaline complex, Yakutia, Russia. *Mineral. Mag.* **1993**, *57*, 651–664. [CrossRef]
35. Dobrovol'skaya, M.G.; Tsepin, A.I.; Evstigneeva, T.L. Murunskite $K_2Cu_3FeS_4$—A new sulfide of potassium, cuprum and iron. *Zapiski Vsesoyuznogo Mineralogicheskogo Obschestva* **1981**, *4*, 468–473.
36. Pekov, I.V.; Zubkova, N.V.; Lisitsyn, D.V.; Pushcharovsky, D.Y. Crystal chemistry of murunskite. *Doklady Earth Sci.* **2009**, *424*, 139–141. [CrossRef]
37. Chakhmouradian, A.R.; Cooper, M.A.; Ball, N.; Reguir, E.P.; Medici, L.; Abdu, Y.A.; Antonov, A.A. Vladykinite, $Na_3Sr_4(Fe^{2+}Fe^{3+})Si_8O_{24}$: A new complex sheet silicate from peralkaline rocks of the Murun complex, eastern Siberia, Russia. *Am. Mineral.* **2014**, *99*, 235–241. [CrossRef]
38. Kostyuk, V.P.; Panina, L.I.; Zhidkov, A.Y.; Orlova, M.P.; Bazarova, T.Y. *Potassic Alkaline Magmatism of the Baikal-Stanovoy Rifting System*; Nauka: Novosibirsk, Russia, 1990; pp. 1–238. ISBN 5-02-028819-5.
39. Wang, Y.; He, H.-Y.; Ivanov, A.V.; Zhu, R.-X.; Lo, C.-H. Age and origin of charoitite, Malyy Murun massif, Siberia, Russia. *Int. Geol. Rev.* **2014**, *56*, 1007–1019. [CrossRef]

40. Ivanov, A.V.; Gorovoy, V.A.; Gladkochub, D.P.; Shevelev, A.S.; Vladykin, N.V. The first precise data on the age of charoite mineralization (Eastern Siberia, Russia). *Doklady Earth Sci.* **2018**, *478*, 179–182. [CrossRef]
41. Donskaya, T.V.; Gladkochub, D.P.; Mazukabzov, A.M.; Ivanov, A.V. Late Paleozoic-Mesozoic subduction-related magmatism at the southern margin of the Siberian continent and the 150 million-year history of the Mongol-Okhotsk Ocean. *J. Asian Earth Sci.* **2013**, *62*, 79–97. [CrossRef]
42. Demonterova, E.I.; Ivanov, A.V.; Mikheeva, E.M.; Arzhannikova, A.V.; Frolov, A.O.; Arzhannikov, S.G.; Bryanskiy, N.V.; Pavlova, L.A. Early to Middle Jurassic history of the southern Siberian continent (Transbaikalia) recorded in sediments of the Siberian Craton: Sm-Nd and U-Pb provenance study. *Bull. Soc. Geol. Fr.* **2017**, *188*. [CrossRef]
43. Stupak, F.M.; Travin, A.V. The age of Late Mesozoic volcanogenic rocks of northern Transbaikalia ($^{40}Ar/^{39}Ar$ data). *Geol. Geofiz.* **2004**, *45*, 280–284.
44. Ripp, G.S.; Izbrodin, I.A.; Doroshkevich, A.G.; Lastochkin, E.I.; Rampilov, M.O.; Sergeev, S.A.; Travin, A.V.; Posokhov, V.F. Chronology of the formation of the gabbro-syenite-granite series of the Oshurkovo pluton, western Transbaikalia. *Petrology* **2013**, *21*, 375–392. [CrossRef]
45. Ivanov, A.V.; Demonterova, E.I.; He, H.-Y.; Perepelov, A.V.; Travin, A.V.; Lebedev, V.A. Volcanism in the Baikal rift: 40 years of active-versus-passive model discussion. *Earth-Sci. Rev.* **2015**, *148*, 18–43. [CrossRef]
46. Dash, B.; Yin, A.; Jiang, N.; Tseveendorj, B.; Han, B. Petrology, structural setting, timing, and geochemistry of Cretaceaous volcanic rocks in eastern Mongolia: Constraints on their tectonic origin. *Gondwana Res.* **2015**, *27*, 281–299. [CrossRef]
47. Ivanov, V.G.; Yarmolyuk, V.V.; Smirnov, V.N. New data on the age of volcanism evidence in the West-Zabaikalian Late Mesozoic-Cenozoic volcanic domain. *Doklady Akademii Nauk* **1995**, *345*, 648–652.
48. Stupak, F.M.; Kudryashova, E.A.; Lebedev, V.A.; Gol'tsman, Y.V. The structure, composition, and conditions of generation for the Early Cretaceous Mongolia-East-Transbaikalia volcanic belt: The Durulgui-Torei area (southern Transbaikalia, Russia). *J. Volcanol. Seismol.* **2018**, *12*, 34–46. [CrossRef]
49. Ponomarchuk, A.V.; Prokopyev, I.R.; Svetlitskaya, T.V.; Doroshkevich, A.G. $^{40}Ar/^{39}Ar$ geochronology of Inagly alkaline rocks (Aldan shield, South Yakutia). *Russ. Geol. Geophys.* **2019**, in press.
50. Shatova, N.V.; Skublov, S.G.; Melnik, A.E.; Shatov, V.V.; Molchanov, A.V.; Terekhov, A.V.; Sergeev, S.A. Geochronology of alkaline magmatic rocks and metasomatites of the Ryabinovy stock (South Yakita) based on zircon isotopic and geochemical (U-Pb, REE) investigations. *Reg. Geol. Met.* **2017**, *69*, 33–48.
51. Polin, V.F.; Glebovitskii, V.A.; Mitsuk, V.V.; Kiselev, V.I.; Budnitskiy, S.Y.; Travin, A.V.; Rizvanov, N.G.; Barinov, N.N.; Ekimova, N.I.; Ponomarchuk, A.V. Two-stage formation of the Alkaline volcano-plutonic complexes in the Ketkap-Yuna igneous province of the Aldan Shield: New isotopic data. *Doklady Earth Sci.* **2014**, *459*, 1322–1327. [CrossRef]
52. Prokoyev, I.R.; Kravchenko, A.A.; Ivanov, A.I.; Borisenko, A.S.; Ponomarchuk, A.V.; Zaitsev, A.I.; Kardash, E.A.; Rozhkov, A.A. Geochronology and ore mineralization of the Dzheltula alkaline massif (Aldan Shield, South Yakutia). *Russ. J. Pac. Geol.* **2018**, *12*, 34–45. [CrossRef]
53. Buchko, I.V.; Sorokin, A.A.; Ponomarchuk, V.A.; Kotov, A.B.; Travin, A.V.; Kovach, V.P. Trachyandesites of the Mogot volcanic field (Stanovoi volcanoplutonic belt, East Siberia): Age, geochemical features, and sources. *Russ. Geol. Geophys.* **2016**, *57*, 1389–1397. [CrossRef]
54. Kiselev, A.I.; Yarmolyuk, V.V.; Ivanov, A.V.; Egorov, K.N. Middle Paleozoic basaltic and kimberlitic magmatism in the northwestern shoulder of the Vilyui Rift, Siberia: Relations in space and time. *Russ. Geol. Geophys.* **2014**, *55*, 144–152. [CrossRef]
55. Steiger, R.H.; Jager, E. Subcommission on geochronology—Convention on use of decay constants in geochronology and cosmochronology. *Earth Planet. Sci. Lett.* **1977**, *36*, 359–362. [CrossRef]
56. Lee, J.-Y.; Marti, K.; Severinghaus, J.P.; Kawamura, K.; Yoo, H.-S.; Lee, J.B.; Kim, J.S. A redetermination of the isotopic abundances of atmospheric Ar. *Geochim. Cosmochim. Acta* **2006**, *70*, 4507–4512. [CrossRef]
57. Min, K.W.; Mundil, R.; Renne, P.R.; Ludwig, K.R. A test for systematic errors in $^{40}Ar/^{39}Ar$ geochronology through comparison with U/Pb analysis of a 1.1 Ga rhyoline. *Geochim. Cosmochim. Acta* **2000**, *64*, 73–98. [CrossRef]
58. Ivanov, A.V. Systematic differences between U-Pb and $^{40}Ar/^{39}Ar$ dates: Reasons and evaluation techniques. *Geochem. Int.* **2006**, *44*, 1041–1047. [CrossRef]

59. Renne, P.R.; Mundil, R.; Balco, G.; Min, K.; Ludwig, K.R. Joint determination of ^{40}K decay constants and ^{40}Ar*/^{40}K for the Fish Canyon sanidine standard, and improved accuracy for ^{40}Ar/^{39}Ar geochronology. *Geochim. Cosmochim. Acta* **2010**, *74*, 5349–5367. [CrossRef]
60. Ivanov, A.V.; Demonterova, E.I.; Savatenkov, V.M.; Perepelov, A.B.; Ryabov, V.V.; Shevko, A.Y. Late Triassic (Carnian) lamproites from Noril'sk, polar Siberia: Evidence for melting of the recycled Archean crust and the question of lamproite source for some placer diamond deposits of the Siberian Craton. *Lithos* **2018**, *296*, 67–78. [CrossRef]
61. Ludwig, K.R. Isoplot 3.75. A geochronological toolkit for Microsoft Excel. *Berkeley Geochronol. Center Spec. Publ.* **2012**, *5*, 1–75.
62. Charoite. Available online: https://www.mindat.org/min-972.html (accessed on 14 November 2018).
63. Lentz, D.R. Carbonaite genesis: A reexamination of the role of intrusion-related pneumatolytic skarn processes in limestone melting. *Geology* **1999**, *27*, 335–338. [CrossRef]